# Measurements of g($4_{1}^{+}$,$2_{2}^{+}$) in $^{70,72,74,76}$Ge: Systematics of low-lying structures in 30≤Z≤40 and 30≤N≤50 nuclei

G. Gürdal, E. A. Stefanova, P. Boutachkov, D. A. Torres, G. J. Kumbartzki, N. Benczer-Koller, Y. Y. Sharon, L. Zamick, S. J. Q. Robinson, T. Ahn, V. Anagnostatou, C. Bernards, M. Elvers, A. Heinz, G. Ilie, D. Radeck, D. Savran, V. Werner, and E. Williams

# Measurements of $g(4_1^+, 2_2^+)$ in $^{70,72,74,76}$Ge: systematics of low-lying structures in $30 \leq Z \leq 40$ and $30 \leq N \leq 50$ nuclei.

G. Gürdal,[1] E. A. Stefanova,[1, *] P. Boutachkov,[1, †] D. A. Torres,[1, ‡] G. J. Kumbartzki,[1] N. Benczer-Koller,[1]
Y. Y. Sharon,[1] L. Zamick,[1] S. J. Q. Robinson,[2] T. Ahn,[3, §] V. Anagnostatou,[3, ¶] C. Bernards,[3, 4]
M. Elvers,[3, 4] A. Heinz,[3, **] G. Ilie,[3] D. Radeck,[3, 4] D. Savran,[3, 5, 6] V. Werner,[3] and E. Williams[3, ††]

[1]*Department of Physics and Astronomy, Rutgers University, New Brunswick, New Jersey 08903, USA*
[2]*Physics Department, Millsaps College, Jackson, Mississippi 39210, USA*
[3]*Wright Nuclear Structure Laboratory, Yale University, New Haven, Connecticut 06511, USA*
[4]*Institut für Kernphysik, Universität zu Köln, D-50937 Köln, Germany*
[5]*ExtreMe Matter Institute EMMI and Research Devision,*
*GSI Helmholtzzentrum für Schwerionenforschung, D-64291 Darmstadt, Germany*
[6]*Frankfurt Institute for Advanced Studies FIAS, D-60348 Frankfurt am Main, Germany*
(Dated: June 12, 2013)

**Background**: The interplay between single-particle and collective excitations in the $30 \leq Z \leq 40$ and $30 \leq N \leq 50$ even-even isotopes has been examined in light of recent new measurements of magnetic moments of $4_1^+$, $2_2^+$ and $2_1^+$ states.

**Purpose**: The $g$ factors of the $4_1^+$ and $2_2^+$ states in the $^{72,74,76}$Ge isotopes have been measured for the first time and the $g(2_1^+)$ values have been remeasured.

**Methods**: The transient field technique (TF) in inverse kinematics with a variety of targets has been applied, following Coulomb excitation of the relevant states. The data have been analyzed within the framework of the IBA-II model. Large-scale shell-model calculations have been performed within the $p_{3/2}, p_{1/2}, f_{5/2}, g_{9/2}$ orbital space for both protons and neutrons with the JUN45 and JJ4B interactions.

**Results**: The measured Ge $g$ factors were compared to the $g$ factors of the low-lying states of the neighboring Zn, Ge, Se, Kr, and Sr isotopes. The results were evaluated in the context of the systematics of $g$ factors in the $A \sim 80$ region.

**Conclusions**: The predictions based on the classic collective model and the Interacting Boson Model IBA-II agree with the experimental results. No evidence for shell closure was found for neutrons at $N = 38$ or $N = 40$.

PACS numbers: 21.10.Ky, 21.60.Cs, 21.60.Ev

## I. INTRODUCTION

Measurements of the magnetic moments of the $2_1^+$ states in most even-even nuclei have provided valuable tests of theoretical models. In particular, such measurements, as a function of neutron or proton number in a chain of nuclei, can highlight features of the interplay between single-particle and collective excitation degrees of freedom. In many cases the details of the wave functions can be elucidated as well. The experimental challenge arises from the difficulty to extend these measurements to $4_1^+$ and $2_2^+$ states. The population, via the Coulomb excitation process, of these states in medium weight nuclei with $30 \leq Z \leq 40$ and $30 \leq N \leq 50$ tends to be of

the order of 100 times smaller than that of the $2_1^+$ state. Furthermore, the alignment of the nuclear spin necessary to observe a precession of the magnetic moment in an external or a hyperfine magnetic field is also much reduced compared to that observed for the $2_1^+$ state.

The Ge nuclei measured in this study are sometimes described in terms of collective vibrational excitations, but they also exhibit characteristics of single-particle excitations.

The four stable even Ge isotopes $^{70,72,74,76}_{32}$Ge$_{38,40,42,44}$ are of special interest for several reasons. One reason is that they span a region of possible sub-shell closure for neutron numbers $N = 38$ or $N = 40$. Another reason stems from the interplay between single-particle and collective excitations. An extensive evaluation of the data available for the $A \sim 80$ region has already been carried out in terms of collective- and shell-model calculations [1] and will be revisited in this paper to include the new data.

The low-lying energy levels of the even-even stable Ge isotopes and the gamma-ray transitions between these levels are shown in Figure 1.

In the simplest spherical shell-model picture for the ground states of the Ge isotopes one could expect the four valence protons beyond the closed $Z = 28$ core to form an inert closed $p_{3/2}$ subshell. As $N$ gradually increases beyond the $N = 28$ closed core, the valence neutrons will first fill the $p_{3/2}$ and $f_{5/2}$ orbitals ending in $^{70}$Ge. The
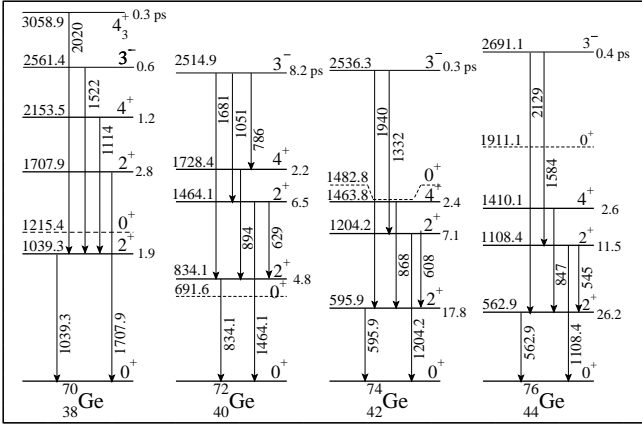
FIG. 1: Partial level schemes for the even-even stable Ge isotopes, showing transisitons observed in this work and the mean lifetimes of the states.



FIG. 2: (Color online) Ratio of experimental excitation energies of $4_1^+$ and $2_1^+$ states in even Ge isotopes and comparison with the results of shell-model calculations using the JUN45 and JJ4B interactions. The line through the experimental points is drawn to guide the eye.

next two neutrons will occupy the $p_{1/2}$ orbital and close the $fp$ shell at $^{72}_{32}Ge_{40}$. As the neutron number increases beyond $N = 40$, the $g_{9/2}$ orbital will gradually fill until it closes at $N = 50$ for $^{82}Ge$.

The above simplified single-particle picture is supported by the measured ground-state spins of $^{69}_{32}Ge_{37}(5/2^-)$, $^{71}_{32}Ge_{39}(1/2^-)$ and $^{73}_{32}Ge_{41}(9/2^+)$. However, the observed ground states spins of $^{67}_{32}Ge_{35}$, $^{75}_{32}Ge_{43}$ (both $1/2^-$) and of $^{77}_{32}Ge_{45}$ $(7/2^+)$ indicate limitations of this perspective.

Other features further challenge the simple shell-model picture. The observed excitation energy of the $2_1^+$ state, about 1 MeV for $N = 34, 36, 38$, drops to 0.83 MeV for $N = 40$ and 0.56 - 0.66 MeV for $N = 42$ - 48. The excitation of the $4_1^+$ state, shows a similar variation with increasing $N$. Fig. 2 shows that this trend is accompanied by a sharp rise in the ratio $E(4_1^+)/E(2_1^+)$ at $N = 42$, but no particular feature at $N = 38$ or 40, where the value of this ratio agrees with the predictions of the vibrational model. The rise from $N = 40$ to 42 suggests the onset of a transition from a collective spherical vibrational description to a more deformed one.

Moreover, the $B(E2; 2_1^+ \to 0_1^+)$ values for the even Ge isotopes with $N = 34$ to 44 range from 12 to 32 W.u. and are larger than the single-particle expectations. They increase monotonically up to $N = 42$ whereas they would be expected to decrease at $N = 38$ or $N = 40$ if a subshell closure were present.

These observations are supported by the experimental $B(E2; 2_1^+ \to 0_1^+)$ values for the entire Zn - Sr region shown in Fig. 3. No obvious discontinuity appears at the boundary of $N = 38$-40. Collectivity becomes significant in Se and further increases in the Kr and Sr nuclei. The magnitude and position of the maxima of the distribution of $B(E2; 2_1^+ \to 0_1^+)$ values as a function of the neutron number shows a clear dependence on the number of protons in the nuclei.

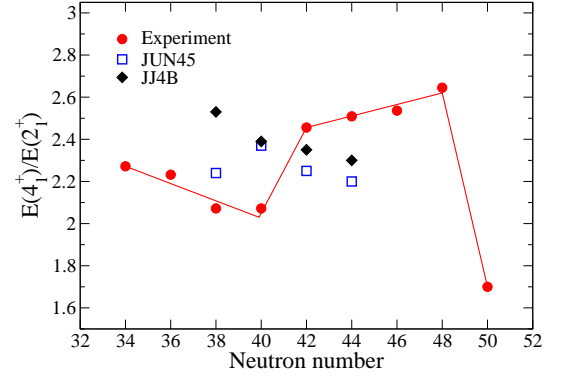The $0_2^+$ excitation energies for the Ge nuclei of interest

exhibit a minimum at $^{72}Ge$ with $N = 40$, where the $0_2^+$ is the first excited state. The $0_2^+$ states in the Ge nuclei were discussed in many references ( [2–5] and references therein) and their behaviour was interpreted as due to both proton and neutron occupations of the $g_{9/2}$ orbitals.

The literature values of the $g(2_1^+)$ of the Ge isotopes have been measured by the integral perturbed angular correlation (IPAC) method and the transient field (TF) techniques both in normal and inverse kinematics and are shown in Table I. In general, the results are in agreement.

Magnetic moments of several higher excited states in Zn, $^{70}Ge$, Se, Kr, Sr and Zr have been measured by the transient field technique [10–17]. However, no such measurements of $g(4_1^+)$ and $g(2_2^+)$ for states in the $^{72,74,76}Ge$ isotopes had been carried out prior to this work.

The present work focused on the measurement of the $g$ factors of the $4_1^+$ and $2_2^+$ states of the four stable $^{70,72,74,76}Ge$ isotopes. At the same time their $g(2_1^+)$ val-
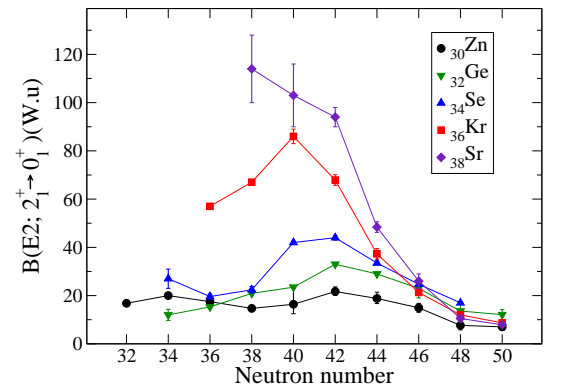


FIG. 3: (Color online) Experimental values of $B(E2; 2_1^+ \to 0_1^+)$ for even nuclei between Zn and Sr. The missing error bars are smaller than the symbols. The experimental data are from Refs. [6, 7] except for $^{70}Se$ [8] and $^{66,68}Ge$ [9] where the more recent results were adopted.

TABLE I: Values of the $g$ factors of $2_1^+$ states in the stable even Ge isotopes obtained in independent measurements and their average value. Ref. [18] is an IPAC measurement while all others are TF measurements.

| $^{70}$Ge | $^{72}$Ge | $^{74}$Ge | $^{76}$Ge | Ref. |
|-----------|-----------|-----------|-----------|------|
| +0.45(10) | +0.35(10) | +0.35(10) | +0.28(6) | [18, 19] |
| +0.470(25) | +0.400(35) | +0.435(20) | +0.420(25) | [20] |
| +0.35(10) | +0.370(45) | +0.350(25) | +0.335(40) | [21] |
| +0.45(10) | | | | [22] |
| +0.42(4) | | | | [11] |
| | | | | |
| +0.45(2) | +0.39(3) | +0.40(2) | +0.38(2) | Average[a] |

[a]Weighted average of all the independent measurements of Refs. [11, 18, 20–22].

TABLE II: Compositions and thicknesses (mg/cm$^2$) of the multilayer targets used in this experiment . The magnetization, $\vec{M}$ at around 80 - 100K, is quoted in Tesla.

| Target | Front | | Ferromagnet | | Backing | | $\vec{M}$[T] |
|--------|-------|-------|-------------|------|---------|------|------|
| | C | Mg[a] | Gd | Fe | Ta | Cu | |
| I | 0.42 | | 3.24 | | 1.4 | 3.51 | 0.172 |
| II | 0.44 | | 3.34 | | 1.4 | 4.49 | 0.186 |
| III | 0.45 | | | 4.44 | | 4.92 | 0.176 |
| IV | | 0.9 | 4.0 | | 1.1 | 3.90 | 0.187 |
| V | | 0.5 | 3.4 | | 1.0 | 5.40 | 0.185 |

[a]Target IV and V contain $^{26}$Mg and $^{24}$Mg, respectively.

ues were remeasured. The results were examined within the larger framework of the systematics of Zn, Ge, Se, Kr and Sr isotopes and compared to the collective $Z/A$ values, the IBA descriptions and to the results of large-scale shell-model calculations.

## II. EXPERIMENTAL TECHNIQUE

The transient field technique, as explained in Ref. [23], was used to measure the $g$ factors. The ions of interest were accelerated by the Tandem at the Wright Nuclear Structure Laboratory at Yale University. Different beam energies were used in an attempt to maximize the excitation of the $4_1^+$ and $2_2^+$ states. However, at energies above the Coulomb barrier (e.g. 194 MeV for $^{70}$Ge on $^{12}$C) competing reaction channels dominate and the Coulomb excitation is suppressed.

The Ge beam ions, which were Coulomb excited and spin aligned in the first layer of the target, traversed the ferromagnetic (gadolinium or iron) layer, where they experienced the hyperfine transient field. After passing the ferromagnetic layer, the Ge nuclei of interest were stopped in a hyperfine-interaction-free copper layer. The tantalum was used as substrate on which gadolinium was evaporated [24]. In Target I a 5 $\mu$g/cm$^2$ titanium flash-
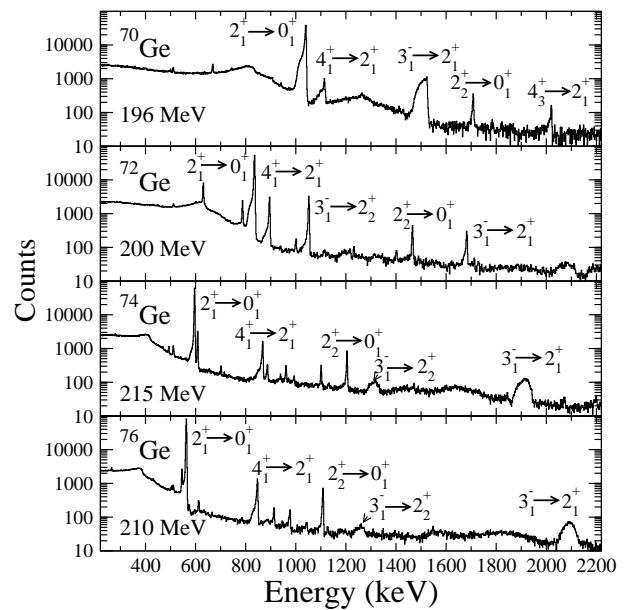


FIG. 4: Partial gamma-ray spectra of the $^{70,72,74,76}$Ge isotopes measured in a backwards clover crystal.

ing was added between the carbon and gadolinium to improve the adherence of these layers. The beam was stopped in an additional thin copper foil placed behind the target, while the knock-on carbon (or magnesium) nuclei had sufficient energy to be detected in a forward-placed particle detector. The targets were cooled to approximately 50K using a closed-cycle refrigerator. The ferromagnetic layer in the target was polarized by an external magnetic field of 0.07 T. The direction of the field was reversed approximately every 120 seconds. The magnetization of the targets was measured with an AC magnetometer [25] as a function of the temperature and was found to be constant in the range of 50K to 120K. The specifics of the different targets used in this work are given in Table II.

The $\gamma$ rays were detected in four clover detectors, each containing four cylindrical, high-purity Ge crystals having a diameter of $\sim$50 mm and a length of $\sim$80 mm. The detectors were placed 120 mm away from the target in the horizontal plane at angles of $\pm$113$°$(detectors 1 and 4) and $\pm$67$°$ (detectors 2 and 3) with respect to the beam direction. Particles were detected about 20 mm downstream of the target either in a conventional 300 mm$^2$, 100 $\mu$m thick silicon surface barrier detector (PIPS) or in a solar-cell detector array consisting of two 15x15 mm or three 10x10 mm Si wafers, joined vertically and framed with a tantalum shield. The choice of the different particle detectors was motivated by the desire to optimize the particle-gamma angular correlations by taking advantage of the slit detector design as explained in Ref. [11].

Table III shows typical kinematics parameters for the different targets and beam energies. The effective transit time, $T$, of the excited ions through the ferromagnetic layer takes into account the decay of short-lived states

TABLE III: Kinematics parameters for the different targets and beam energies for the $2_1^+$ state for each isotope. The $< E >_{\mathrm{in}}$ and $< E >_{\mathrm{out}}$, and $< v/v_0 >_{\mathrm{in}}$ and $< v/v_0 >_{\mathrm{out}}$, are, respectively, the average energies and velocities of the excited ions as they enter into, and exit from, the ferromagnetic layer and $v_0 = e^2/\hbar$ is the Bohr velocity. $T$ is the effective transit time of the ions through the ferromagnetic layer.

| Probe ions | Target | $E_{\mathrm{beam}}$ (MeV) | $< E >_{\mathrm{in}}$ (MeV) | $< E >_{\mathrm{out}}$ (MeV) | $< \frac{v}{v_0} >_{\mathrm{in}}$ | $< \frac{v}{v_0} >_{\mathrm{out}}$ | $T$ (ps) |
|---|---|---|---|---|---|---|---|
| $^{70}$Ge | I | 190 | 87.6 | 38.5 | 7.1 | 4.7 | 0.287 |
| | I | 225 | 111.3 | 57.3 | 8.0 | 5.8 | 0.258 |
| | II | 196 | 91.2 | 39.1 | 7.3 | 4.8 | 0.307 |
| | IV | 225 | 49.8 | 8.8 | 5.4 | 1.9 | 0.521 |
| $^{72}$Ge | I | 190 | 89.1 | 40.0 | 7.1 | 4.7 | 0.308 |
| | II | 200 | 96.6 | 44.4 | 7.4 | 5.0 | 0.304 |
| | IV | 200 | 35.6 | 4.9 | 4.5 | 1.7 | 0.768 |
| $^{74}$Ge | I | 190 | 90.5 | 41.5 | 7.0 | 4.8 | 0.319 |
| | II | 165 | 77.2 | 30.7 | 6.5 | 4.1 | 0.368 |
| | II | 180 | 83.8 | 35.3 | 6.8 | 4.4 | 0.348 |
| | II | 190 | 89.3 | 39.3 | 7.0 | 4.6 | 0.334 |
| | II | 200 | 94.8 | 43.5 | 7.2 | 4.9 | 0.320 |
| | II | 215 | 106.6 | 52.7 | 7.6 | 5.4 | 0.299 |
| | III | 190 | 90.4 | 6.7 | 7.0 | 1.9 | 0.608 |
| | V | 215 | 57.2 | 17.3 | 5.6 | 3.1 | 0.768 |
| $^{76}$Ge | I | 190 | 92.7 | 43.5 | 7.0 | 4.8 | 0.319 |
| | II | 210 | 103.1 | 50.3 | 7.4 | 5.2 | 0.309 |
| | III | 200 | 102.1 | 8.3 | 7.4 | 2.1 | 0.598 |
| | IV | 200 | 38.8 | 6.3 | 4.5 | 1.8 | 0.812 |

while traversing the ferromagnetic layer.

## III. ANALYSIS AND RESULTS

The energy and timing information for each single $\gamma$-ray and particle event was obtained directly from the preamplifier signals of the detectors using Pixie-4 pulse digitizers [26] and was written to disk. Particle-gamma coincidences were later selected from time-difference spectra. Compton add-back was performed for each individual crystal in a clover detector. Particle-gamma ray coincidence spectra for the $^{70,72,74,76}$Ge isotopes, obtained in one crystal of a clover, are shown in Fig. 4. The $2_1^+ \rightarrow 0_1^+$ transition is the dominant feature in all spectra. The excitation of the $2_2^+$ and $4_1^+$ states, even at the higher beam energies, is less than 5% of that of the $2_1^+$ state. At beam energies near and above the Coulomb barrier the excitation of the $3_1^-$ state increases more rapidly. If the $3_1^-$ decay feeds into the lower-lying $2_2^+$ and $4_1^+$ states then their $g$-factor analysis becomes more complicated.

The experimental precession angle, $\Delta\theta^{\mathrm{exp}}$, was obtained from small rate changes in the spectra recorded by the $\gamma$-ray detectors for the alternating magnetic field directions at the target. The $\gamma$-ray peak intensities for the measured transitions, observed in each detector ($i,j = 1,2,3,4$) for each field direction, were used to form double ratios,

$$\rho = \sqrt{\rho_{1,4}/\rho_{2,3}} \quad \text{where} \quad \rho_{\mathrm{i,j}} = \sqrt{(\mathrm{N}_i^\uparrow/\mathrm{N}_i^\downarrow)/(\mathrm{N}_j^\uparrow/\mathrm{N}_j^\downarrow)} \tag{1}$$

from which the effect $\varepsilon = (\rho - 1)/(\rho + 1)$ was calculated. In this procedure unknown quantities, like differences in the up/down measurement times and relative efficiencies of the detectors, cancel. This effect $\varepsilon$ needs to be converted into a precession angle through the relation $\Delta\theta^{exp} = \varepsilon/S(\theta)$.

The logarithmic slope, $S(\theta) = \frac{1}{W(\theta)}\frac{dW(\theta)}{d\theta}$, was obtained from the measured particle-$\gamma$ correlation

$$W(\theta) = 1 + A_2^{\mathrm{exp}}P_2(\cos\theta) + A_4^{\mathrm{exp}}P_4(\cos\theta). \tag{2}$$

The $P_k(\cos\theta)$ are Legendre polynomials of order $k$ and the $A_k^{\mathrm{exp}}$ are the angular correlation coefficients, which depend on the multipolarity of the $\gamma$-ray transition and the geometry of the particle and $\gamma$ detectors.

The transient field strength, $B_{TF}(v(t), Z)$, was calculated using the Rutgers parametrization [23] and the expression

$$\Delta\theta^{\mathrm{calc}}(g = 1) = \frac{\mu_N}{\hbar}\int_{t_{\mathrm{in}}}^{t_{\mathrm{out}}} B_{TF}(v(t), Z)e^{-t/\tau}dt. \tag{3}$$

Table IV shows the slopes, $\Delta\theta^{\mathrm{exp}}$, $\Delta\theta^{\mathrm{calc}}(g = 1)$ and the $g$ factors obtained using different targets and beam

energies. Only the $2_2^+ \to 0_1^+$ transition was used in the determination of the $g$ factor of the $2_2^+$ state. The errors assigned to the $g$ factors of the $4_1^+$ and $2_2^+$ are predominantly statistical.

The measurements were carried out over a period of several years with remarkable reproducibility. But it was also found that for different targets the results showed systematic differences, which could not be explained by the target parameters or kinematic differences in the experiments. The measurements on the magnesium targets resulted in systematically smaller values (about 15% for Target IV and 30% for Target V) for the absolute $g$ factors. No reasonable explanation for the difference in the results was found. The magnesium ions have lower energies when scattered at larger angles and may fall below the detection threshold. But measurements with a reduced opening angle for the magnesium particle detection confirmed the results. The target parameters were confirmed when the same magnesium targets were used with Kr, Ru or Mo beams and gave results in agreement with corresponding measurements obtained with carbon targets. Nevertheless, based on the assumption that the relative $g$-factor results are independent of the transient field parameters, the $4_1^+$ and $2_2^+$ measurements with the magnesium targets were included in Table IV after the $\Delta\theta(g=1)$ calculations were scaled to match the average $2_1^+$ carbon target data.

### A. $^{70}$Ge

The $g$ factors of the $2_1^+$, $4_1^+$ and $3_1^-$ states of $^{70}$Ge were already published in [11]. During the course of this work, the $g$ factor of the $(2_1^+)$ state in $^{70}$Ge was remeasured using Target II and the literature value ([11]) was reproduced. The observed $2_2^+ \to 0_1^+$ $\gamma$-ray transition in this work indicates that the mean life of of this state is longer than 1.6 ps quoted in Ref. [7]. A more recent measurement [22] yielded $\tau(2_2^+) = 2.8(4)$ ps, which was used in this work. Due to the low statistics, the $g(2_2^+)$ factor has a large error. No feeding from the $3_1^-$ state to the $4_1^+$ or $2_2^+$ states was observed.

### B. $^{72}$Ge

The $3_1^-$ state in $^{72}$Ge, unlike in the other Ge isotopes, has a relatively long lifetime of 8.2 ps and is strongly excited at the beam energy of 200 MeV. Its decay populates the $2_2^+$ state to 70% and the $4_1^+$ state to 25%. The $g$ factor of the $3_1^-$ state is unknown and cannot be derived with reasonable precision from this experiment: the $\gamma$ detectors are not at optimal angles for dipole transitions, the slopes could not be determined accurately and the $3_1^- \to 0_1^+$ transition is very weak.

Because of the long lifetime of the $3_1^-$ state the feeding into the $2_2^+$ and $4_1^+$ states carries the full contribution of the $g(3_1^-)$ factor. Given the large errors of the measured

$g$ factors a feeding correction, as outlined in Ref. [11], was not attempted. Assuming a possible range of values for the $g(3_1^-)$ factor between 0.4 and 0.6 would not change the measured values beyond their errors. Therefore, the quoted $g(2_2^+)$ and $g(4_1^+)$ values in Table IV are stated as measured. The measured slopes of the $2_2^+ \to 0_1^+$ and $4_1^+ \to 2_1^+$ transitions include the $3_1^-$ feeding as an unobserved contribution to the angular correlation.

### C. $^{74}$Ge

Extensive measurements were carried out on $^{74}$Ge over a wide range of energies, employing all available particle-detectors and targets. The results in Table IV for the $2_1^+$ state also demonstrate the dependence of the slopes on the particle-detector geometry and beam energy. In the experiments with Targets I and III the circular PIPS detector was used. The "slit" geometry of the solar-cell array used with Target II gives larger slopes but also shows a decrease of the slopes at the higher beam energies. At and above the Coulomb barrier the slope is reduced due to a diminished alignment and to increased feeding from the $3_1^-$ state. In the experiment using Target V at 215 MeV a vertically-mounted triple solar-cell array was used as particle detector. The center cell at zero degrees had an opening angle of $\pm 9^\circ$, each cell above and below covered $11^\circ - 29^\circ$. The measured slopes for the $2_1^+ \to 0_1^+$ transition for the center and peripheral detectors, $S(67^\circ)_{center} = -2.457(24)$ and $S(67^\circ)_{peripheral} = -2.493(22)$, were, within errors, the same.

The $3_1^-$ state has a very short lifetime of 0.3 ps. The $\gamma$-ray line is Doppler broadened and fully shifted. There is feeding to the $2_2^+$ state at 215 MeV but little feeding was observed at the lower beam energies. No feeding correction was applied to the $g(2_2^+)$ factor and no feeding path to the $4_1^+$ state was observed.

### D. $^{76}$Ge

At 210 MeV the $3_1^-$ state is excited. As in $^{74}$Ge the $\gamma$-ray line is fully shifted in accordance with a lifetime of 0.4 ps. No feeding of the $4_1^+$ state was observed and no feeding corrections were applied to the data in Table IV. The $4_1^+ \to 2_1^+$ transition has the same energy, 847 keV, as the $2_1^+ \to 0_1^+$ in iron and therefore the $g(4_1^+)$ could not be extracted from the iron target data.

## IV. MODELS AND CALCULATIONS

In the present investigation, the $g$ factors of $2_1^+$, $4_1^+$ and $2_2^+$ excited states of the stable even $_{32}$Ge nuclei were measured. The results were compared to the corresponding $g$ factors in the neighboring $_{30}$Zn, $_{34}$Se, $_{36}$Kr, and $_{38}$Sr isotopes. These region-wide data were analyzed in

TABLE IV: Summary of experimental results from this work including the slopes of the angular correlations and the calculated precession $\Delta\Theta^{\mathrm{calc}}(g=1)$.

| Nucleus | $I^\pi$ | $\tau$ ps | Target | $E_{\mathrm{beam}}$ MeV | $|S(67^\circ)|$ (mrad$^{-1}$) | $|\Delta\theta^{\mathrm{exp}}|$ (mrad) | $\Delta\Theta^{\mathrm{calc}}(g=1)$ (mrad) | $g$ this work | $<g>$ |
|---|---|---|---|---|---|---|---|---|---|
| $^{70}$Ge | $2^+_1$ | 1.9 | II | 196 | 2.35(2) | 11.0(7) | 25.2 | +0.44(4) | +0.44(4) |
| | $2^+_2$ | 2.8 | I | 225 | 1.68(1) | 8.6(82) | 22.2 | +0.39(37) | +0.66(28) |
| | | | II | 196 | 1.77(16) | 27.5(117) | 26.7 | +1.03(44) | |
| | $4^+_1$ | 1.2 | II | 196 | 0.86(9) | 6.1(183) | 23.1 | +0.21(63) | +0.22(31) |
| | | | IV | 225 | 0.84(3) | 5.5(88) | 24.6 | +0.22(36) | |
| $^{72}$Ge | $2^+_1$ | 4.8 | I | 190 | 1.96(1) | 12.6(8) | 24.7 | +0.51(4) | +0.44(2) |
| | | | II | 200 | 2.18(2) | 10.6(5) | 26.9 | +0.40(3) | |
| | $2^+_2$ | 6.5 | I | 190 | 1.64(1) | 4.6(104) | 24.9 | +0.19(42) | +0.42(21) |
| | | | II | 200 | 1.320(4) | 4.6(132) | 26.9 | +0.17(49) | |
| | | | IV | 200 | 1.399(8) | 23.8(88) | 40.6 | +0.59(27) | |
| | $4^+_1$ | 2.2 | I | 190 | 0.754(3) | 14.2(164) | 23.3 | +0.61(70) | +0.39(13) |
| | | | II | 200 | 0.814(3) | 4.6(79) | 25.2 | +0.18(31) | |
| | | | IV | 200 | 0.814(8) | 14.2(46) | 33.2 | +0.43(14) | |
| $^{74}$Ge | $2^+_1$ | 17.8 | I | 190 | 1.96(1) | 10.3(5) | 25.5 | +0.40(3) | +0.35(1) |
| | | | II | 165 | 2.66(1) | 10.1(67) | 30.3 | +0.33(3) | |
| | | | II | 180 | 2.642(9) | 9.2(4) | 29.2 | +0.32(2) | |
| | | | II | 200 | 2.596(8) | 10.2(4) | 27.9 | +0.36(2) | |
| | | | II | 215 | 2.177(8) | 10.0(4) | 26.9 | +0.37(2) | |
| | | | III | 190 | 1.98(1) | 12.9(6) | 39.3 | +0.33(2) | |
| | $2^+_2$ | 7.1 | I | 190 | 1.64(1) | 10.5(102) | 25.0 | +0.42(41) | +0.47(10) |
| | | | II | 180 | 2.32(26) | 3.9(79) | 28.6 | +0.14(28) | |
| | | | II | 200 | 1.85(8) | 17.6(58) | 27.3 | +0.65(22) | |
| | | | II | 215 | 1.47(8) | 21.0(56) | 26.6 | +0.79(21) | |
| | | | III | 190 | 1.71(8) | 18.4(130) | 38.2 | +0.48(34) | |
| | | | V | 180 | 2.33(2) | 11.3(91) | 26.7 | +0.42(34) | |
| | | | V | 200 | 2.13(11) | 15.8(88) | 24.5 | +0.64(36) | |
| | | | V | 215 | 2.01(14)[a] | 4.3(111) | 23.3 | +0.19(36) | |
| | | | V | 215 | 2.30(13)[b] | −4.3(90) | 24.7 | −0.18(36) | |
| | $4^+_1$ | 2.4 | II | 180 | 1.23(16) | 14.2(107) | 26.4 | +0.54(41) | +0.40(12) |
| | | | II | 200 | 0.93(3) | 14.4(62) | 25.9 | +0.59(25) | |
| | | | II | 215 | 0.86(5) | 15.2(62) | 25.4 | +0.62(25) | |
| | | | III | 190 | 0.90(5) | 12.0(130) | 34.8 | +0.35(38) | |
| | | | V | 180 | 1.12(12) | −4.2(71) | 22.9 | −0.18(34) | |
| | | | V | 200 | 0.99(1) | 1.5(106) | 21.9 | +0.07(48) | |
| | | | V | 215 | 0.97(13)[a] | −7.5(106) | 22.0 | −0.36(50) | |
| | | | V | 215 | 0.91(12)[b] | 13.8(78) | 21.0 | +0.63(36) | |
| $^{76}$Ge | $2^+_1$ | 26.2 | I | 190 | 1.94(1) | 10.0(6) | 25.5 | +0.39(3) | +0.32(1) |
| | | | II | 210 | 2.42(2) | 8.7(2) | 27.4 | +0.32(2) | |
| | | | III | 200 | 2.19(2)[c] | 13.3(9) | 42.5 | +0.32(1) | |
| | | | III | 200 | 2.63(2)[d] | 13.1(3) | 42.5 | +0.31(1) | |
| | $2^+_2$ | 11.5 | I | 190 | 1.64(1) | 10.9(84) | 25.2 | +0.43(33) | +0.39(5) |
| | | | II | 210 | 2.05(3) | 7.8(27) | 27.1 | +0.29(10) | |
| | | | III | 200 | 1.20(13)[c] | 20.8(135) | 41.4 | +0.50(32) | |
| | | | III | 200 | 2.16(8)[d] | 15.2(42) | 41.9 | +0.36(10) | |
| | | | IV | 200 | 1.98(6) | 18.1(26) | 41.6 | +0.44(7) | |
| | $4^+_1$ | 2.6 | I | 190 | 0.90(5) | 2.6(131) | 23.6 | +0.11(56) | +0.24(17) |
| | | | II | 210 | 0.87(9) | 6.7(47) | 25.4 | +0.26(18) | |
| | | | IV | 200 | 0.95(4) | 4.9(34) | 34.0 | +0.12(86) | |

[a]Vertically-mounted three solar-cell array: center cell
[b]Vertically-mounted three solar-cell array: top and bottom cells
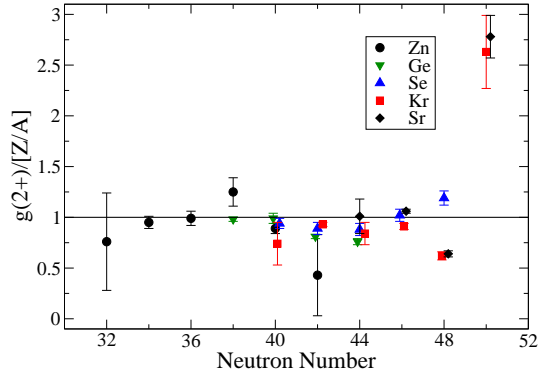[c]Cylindrical particle detector
[d]Rectangular solar-cell detector

FIG. 5: (Color online) Measured $g(2_1^+)$ factors compared to $Z/A$. The average value, excluding the $N = 50$ nuclei, is $<g(2_1^+)> = + 0.84(1)$ [Z/A].
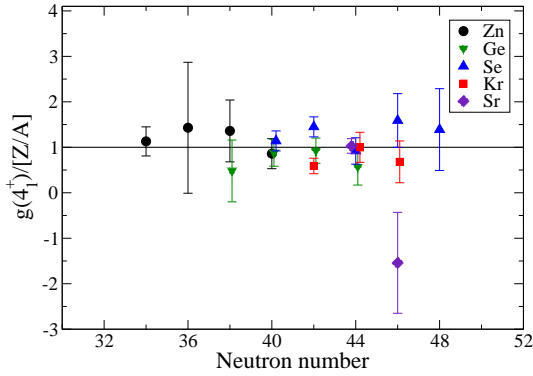


FIG. 6: (Color online) Measured $g(4_1^+)$ factors compared to $Z/A$. The average value is $<g(4_1^+)> = + 0.97(7)$ [Z/A]. The value $g(^{86}Sr;4_1^+)$ is indeed negative [27] and does not conform to the value expected for a collective excitation.
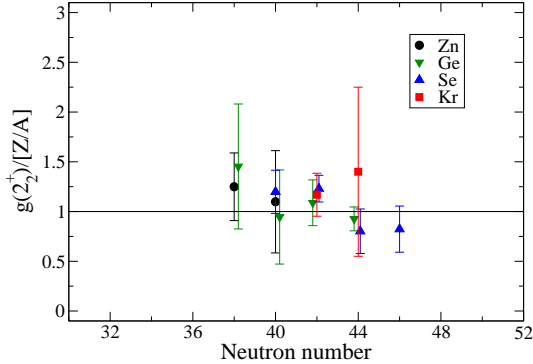


FIG. 7: (Color online) Measured $g(2_2^+)$ factors compared to $Z/A$. The average value is $<g(2_2^+)> = + 0.95(7)$ [Z/A].

terms of the classic collective and the IBA models. Subsequently, large-scale shell-model calculations were carried out to understand the microscopic structure of the low-lying states of the four Ge isotopes.

## A. Collective models

In the classic collective model of Bohr and Mottelson, all $g$ factors of the sequential states in a band have $g$ factors equal to $Z/A$. The data for the $2_1^+$, $4_1^+$ and $2_2^+$ states in isotopes of Zn, Ge, Se, Kr, Sr have been compared to this prediction in Figs. 5, 6 and 7, respectively. The $g(2_1^+)$ values, on average, lie below $Z/A$, while the averages of all the $g(4_1^+)$ and $g(2_2^+)$ values agree well with the $Z/A$ prediction. No particular deviation from a smooth distribution is observed near the "semi-magic" numbers of $N = 38,40$.

A different approach, provided by the interacting boson model [28, 29], can be considered. Sambataro [30], using the formulation of Morrison [31], expressed the $g$ factor of the $2_1^+$ state in terms of the number of valence proton bosons, $N_\pi$, valence neutron bosons, $N_\nu$, and the effective $g$ factors of proton and neutron bosons, $g_\pi$ and $g_\nu$, respectively

$$g(2_1^+)(\frac{N_{tot}}{N_\nu}) = g_\pi(\frac{N_\pi}{N_\nu}) + g_\nu, \qquad (4)$$

where $N_{tot} = N_\pi + N_\nu$.

This analysis for the $2_1^+$ states was presented previously in Refs. [1, 13] and is reproduced here with the inclusion of new data. The same formalism was extended here to the data for $g(4_1^+)$ and $g(2_2^+)$. The results are presented in Figs. 8, 9 and 10. The $g$ factors are compared to the IBA-II descriptions for cases where $N = 28$, 38, 50 and $Z = 28$, 50 correspond to closed shells. Only the data for the $N = 48$ nuclei (two neutrons away from the closed $N = 50$ shell) deviate from the linear trend. The data for $N = 38$, 48 were not included in the fit. The specific magic numbers for $N$ and $Z$ were chosen because they yielded the best $\chi^2$ to a straight-line fit in the analysis of Ref. [1]. Although there are fewer $g$-factor data for the higher excited states and they have relatively larger errors, the data also exhibit a linear dependence on $N_\pi/N_\nu$. Indeed, a straight line with the same effective boson-proton and boson-neutron $g$ factors, $g_\pi$ and $g_\nu$, fits all three data sets. A representation of the data in terms of $N_\pi N_\nu/N_{tot}$ did not display any deviations from a smooth distribution.

## B. Shell-model calculations

Large-scale shell-model calculations [2] had been carried out for $^{70,72,74,76}$Ge using the $p_{3/2}$, $f_{5/2}$ $p_{1/2}$ and $g_{9/2}$ model space for both protons and neutrons and two interactions, JUN45 [3] and JJ4B [32].

The excitation energies, $B(E2; 2_1^+ \to 0_1^+)$, $B(E2; 4_1^+ \to 2_1^+)$, $B(E2; 2_2^+ \to 2_1^+)$, $B(E2; 2_2^+ \to 0_1^+)$ values and static quadrupole moments of the $2_1^+$, $2_2^+$ and $4_1^+$ states were calculated for each nucleus. The excitation energies were in reasonable agreement with the experimental data. However, the quadrupole moments of the $2_1^+$ states
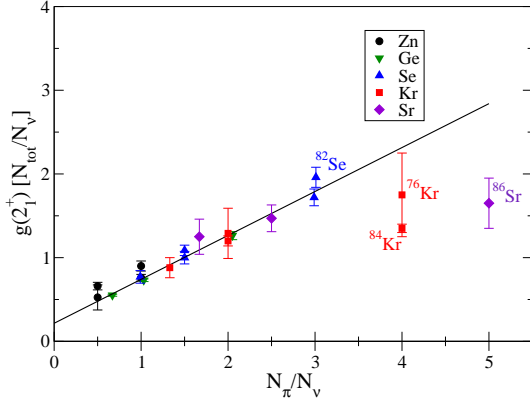
FIG. 8: (Color online) Experimental values of $g(2_1^+)(N_{tot}/N_\nu)$ for the case of neutron shell closure at $N = 38$ and for $28 < Z < 50$. The best fit to a linear distribution yields values for the valence proton and neutron boson $g$ factors of $g_\pi = +0.511(21)$, and $g_\nu = +0.216(20)$.
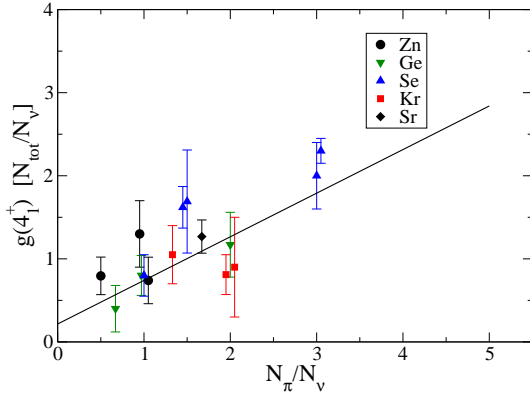


FIG. 9: (Color online) Experimental values of $g(4_1^+)(N_{tot}/N_\nu)$ for the case of neutron shell closure at $N = 38$ and $28 < Z < 50$. The solid line has the same parameters as the best fit for the $g(2_1^+)$ data.
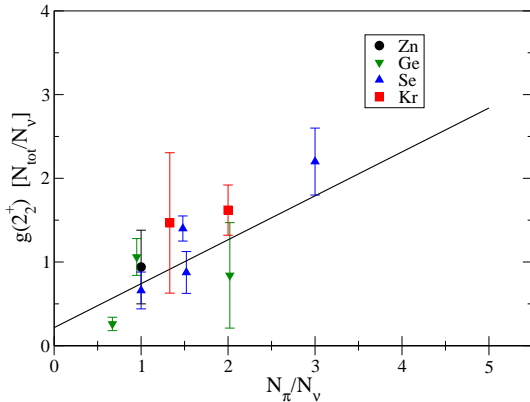


FIG. 10: (Color online) Experimental values of $g(2_2^+)(N_{tot}/N_\nu)$ for the case of neutron shell closure at $N = 38$ and $28 < Z < 50$. The solid line is the same as in Fig. 8.

were not well accounted for by the shell-model calculations [2].

These observations suggest that the shell-model calculation used an incomplete set of valence states and lend weight to the consideration of collective behavior.

The present work extends the shell-model calculations of Ref. [2] to include $g$ factors. In addition, it discusses for each state the detailed shell-model wave functions and also the average occupation numbers of protons and neutrons in each shell-model orbital. Typically, each wave function involves twenty or more shell-model configurations, each with a probability of more than 1%. There is no single configuration in any wave function with a probability of more than 20%. Overall, for each of the specific nuclear states, the leading configurations and their probabilities are similar for the JUN45 and JJ4B interactions. Also similar for each specific state are the results obtained with both interactions for the occupation numbers of the single-particle proton and neutron orbitals. For any one nucleus, with either interaction, the average orbital occupancies for the $0_1^+$, $2_1^+$, $2_2^+$, $4_1^+$ states are almost identical. Thus, for each nucleus, for a given interaction, the wave functions are highly fractionated and exhibit no sharp structural effects.

One would have expected that in all four Ge isotopes the four valence protons beyond $Z = 28$ occupy the $p_{3/2}$ sub-shell, filling it up completely. In such a simple picture, the protons would be inert. However, with both interactions for all four nuclei and for all four states, the occupancies of the $p_{3/2}$ orbital range only from 1.44 to 2.28. The other valence protons are mostly in the $f_{5/2}$ shell with occupancies ranging from 0.96 to 2.08. The occupancy of the $p_{1/2}$ proton orbital is always less than 0.54. The occupancies of protons in the $g_{9/2}$ orbital are low and always smaller than 0.36. Thus the calculation suggests that proton excitations to the $g_{9/2}$ orbits play only a minor role, contrary to what was found in Ref. [4].

On the basis of the simplest shell model no neutrons would be expected to occupy the $(g_{9/2})_\nu$ orbital in the ground state for $^{70}$Ge and $^{72}$Ge as the neutron $fp$ shell closes. Two $g_{9/2}$ neutrons would be expected for $^{74}$Ge and four for $^{76}$Ge. The large-scale shell-model calculations however indicate earlier and greater average neutron $(g_{9/2})_\nu$ occupancies. For the JJ4B interaction this average occupancy is about 2.6 for $^{70}$Ge, 3.9 for $^{72}$Ge, 5.1 for $^{74}$Ge and 6.2 for $^{76}$Ge. For the JUN45 interaction the corresponding numbers are 2.1, 3.3, 4.5 and 5.9. The average total number of holes in the $p_{3/2}$, $f_{5/2}$ and $p_{1/2}$ orbitals decreases as $N$ increases from 38 ($^{70}$Ge) to 44 ($^{76}$Ge). The simple shell model predicts two such holes in $^{70}$Ge and none in the heavier Ge nuclei. The actual number of total holes as $N$ increases is 4.6, 3.9, 3.2 and 2.2 for JJ4B and 4.1, 3.3, 2.5 and 1.9 for JUN45. With both interactions the largest number of holes are in the $f_{5/2}$ orbital. The average number of $f_{5/2}$ holes as $N$ increases is respectively 2.6, 2.1, 1.7 and 1.3 with JJ4B and 2.3, 1.8, 1.3 and 0.9 with JUN45. It is thus seen that typically in the calculation with the JJ4B interaction more

TABLE V: Comparison of experiment and theory. The $g(2_2^+)$ data are the experimental results from this work combined with the compilation of Table I. The data are compared with theoretical predictions of the collective model ($Z/A$) and of two shell-model calculations using free and effective proton and neutron $g$ factors with $g_{s(\text{eff})} = 0.7 g_{s(\text{free})}$.

| Isotope | $g_{\text{exp}}$ | $Z/A$ | Shell Model[a] | | |
| --- | --- | --- | --- | --- | --- |
| | | | JJ4B$_{\text{free}}$ | JUN45$_{\text{free}}$ | JUN45$_{\text{eff}}$ |
| $2_1^+$ | | | | | |
| $^{70}$Ge | +0.449(18) | +0.46 | + 0.272 | +0.342 | +0.355 |
| $^{72}$Ge | +0.421(16) | +0.44 | + 0.228 | +0.271 | +0.304 |
| $^{74}$Ge | +0.365(8) | +0.43 | + 0.260 | +0.247 | +0.289 |
| $^{76}$Ge | +0.330(7) | +0.42 | + 0.235 | +0.304 | +0.347 |
| $4_1^+$ | | | | | |
| $^{70}$Ge | +0.36(21)[b] | +0.46 | +0.259 | +0.299 | +0.328 |
| $^{72}$Ge | +0.39(13) | +0.44 | +0.134 | +0.236 | +0.276 |
| $^{74}$Ge | +0.40(12) | +0.43 | +0.180 | +0.152 | +0.206 |
| $^{76}$Ge | +0.24(17) | +0.42 | +0.160 | +0.229 | +0.286 |
| $2_2^+$ | | | | | |
| $^{70}$Ge | +0.66(28) | +0.46 | +0.538 | +0.647 | +0.626 |
| $^{72}$Ge | +0.42(21) | +0.44 | +0.472 | +0.636 | +0.627 |
| $^{74}$Ge | +0.47(10) | +0.43 | +0.437 | +0.570 | +0.576 |
| $^{76}$Ge | +0.39(5) | +0.42 | +0.480 | +0.513 | +0.497 |

[a]In the $g$-factor calculations for $^{70,72}$Ge the maximum number of protons in the $g_{9/2}$ orbital was limited to 2.
[b]Includes value in Ref. [11]

$f_{5/2}$ neutrons are excited to the $g_{9/2}$ orbital than in the calculation using the JUN45 interaction. The number of neutron holes in the $fp$ shell in this large-scale shell-model calculation indicates that there are no rigid shell closures at $N = 38$ or $N = 40$. The neutron excitations to the $g_{9/2}$ would be expected to increase $B(E2)$ values and perhaps decrease $g$-factor values.

The results of the shell-model calculations of $g$ factors are presented in Table V. The results are in general agreement with the observed values of the $g$ factors of the $2_2^+$ states, within their errors, but tend to underestimate the $g$ factors of the $2_1^+$ and $4_1^+$ states. The simple collective estimate of $Z/A$ is in better agreement with the data.

## V. SUMMARY

New measurements of $g(2_1^+, 4_1^+, 2_2^+)$ have been carried out in the $^{70,72,74,76}$Ge isotopes. Predictions based on simple collective models and the Interacting Boson Model IBA-II yield good agreement with the data analysis in the region discussed in Ref. [1] and with the new measurements presented in the present paper. No evidence was found for neutron shell closures at $N = 38$ or $N = 40$. New shell-model calculations with a large basis including $g_{9/2}$ orbitals yield very fractionated wave functions and probably indicate an incomplete set of basis states. In conclusion, this particular region spanning nuclei between Zn and Sr requires a wider theoretical framework than that provided so far.

[1] T. J. Mertzimekis, A. E. Stuchbery, N. Benczer-Koller, and M. J. Taylor, Phys. Rev. C **68**, 054304 (2003).

[2] S. J. Q. Robinson, L. Zamick, and Y. Y. Sharon, Phys. Rev. C **83**, 027302 (2011).

[3] M. Honma, T. Otsuka, T. Mizusaki, and M. Hjorth-Jensen, Phys. Rev. C **80**, 064323 (2009).

[4] M. Hasegawa, T. Mizusaki, K. Kaneko, and Y. Sun, Nucl. Phys. **A 789**, 46 (2007).

[5] M. Honma, T. Otsuka, T. Mizusaki, and M. Hjorth-Jensen, Journal of Physics: Conference Series **49**, 45 (2006).

[6] S. Raman, C. W. Nestor, Jr., and P. Tikkanen, Atomic Data and Nuclear Data Tables **78**, 1 (2001).

[7] ENDSF: `http://www.nndc.bnl.gov/nndc/ensdf/`.

[8] J. Ljungvall, A. Görgen, M. Girod, J.-P. Delaroche, A. Dewald, C. Dossat, E. Farnea, W. Korten, B. Melon, R. Menegazzo, et al., Phys. Rev. Lett. **100**, 102502 (2008).

[9] R. Lüttke, E. A. McCutchan, V. Werner, K. Aleksandrova, S. Atwater, H. Ai, R. J. Casperson, C. R. F., A. Heinz, A. F. Mertz, et al., Phys. Rev. C **85**, 017301 (2012).

[10] D. Mücher, G. Gürdal, K.-H. Speidel, G. J. Kumbartzki, N. Benczer-Koller, S. J. Q. Robinson, Y. Y. Sharon, L. Zamick, A. F. Lisetskiy, R. J. Casperson, et al., Phys. Rev. C **79**, 054310 (2009).

[11] P. Boutachkov, S. J. Q. Robinson, A. Escuderos, G. Kumbartzki, N. Benczer-Koller, E. Stefanova, Y. Y. Sharon, L. Zamick, E. A. McCutchan, V. Werner, et al., Phys. Rev. C **76**, 054311 (2007).

[12] K.-H. Speidel, N. Benczer-Koller, G. Kumbartzki, C. Barton, A. Gelberg, J. Holden, G. Jakob, N. Matt, R. H. Mayer, M. Satteson, et al., Phys. Rev. C **57**, 2181 (1998).

[13] T. J. Mertzimekis, N. Benczer-Koller, J. Holden, G. Jakob, G. Kumbartzki, K.-H. Speidel, R. Ernst, A. Macchiavelli, M. McMahan, L. Phair, et al., Phys. Rev. C **64**, 024314 (2001).

[14] A. I. Kucharska, J. Billowes, and M. A. Grace, J. Phys. **G 14**, 65 (1988).

[15] G. Jakob, N. Benczer-Koller, J. Holden, G. Kumbartzki, T. J. Mertzimekis, K.-H. Speidel, C. W. Beausang, and R. Krücken, Phys. Lett. **B468**, 13 (1999).

[16] G. Jakob, N. Benczer-Koller, J. Holden, G. Kumbartzki, T. J. Mertzimekis, K.-H. Speidel, R. Ernst, P. Maier-Komor, C. W. Beausang, and R. Krücken, Phys. Lett. **B494**, 187 (2000).

[17] G. Kumbartzki, N. Benczer-Koller, J. Holden, G. Jakob, T. J. Mertzimekis, M. J. Taylor, K.-H. Speidel, R. Ernst, A. E. Stuchbery, C. W. Beausang, et al., Phys. Lett. **B562**, 193 (2003).

[18] C. Fahlander, K. Johansson, E. Karlsson, and G. Possnert, Nucl. Phys. **A 291**, 241 (1977).

[19] N. J. Stone, IAEA (2011).

[20] A. Pakou, J. Billowes, J. A. G. D. Raedt, M. A. Grace, and W. R. Kölbl, J. Physics G **10**, 1759 (1984).

[21] G. J. Lampard, H. H. Bolotin, A. E. Stuchbery, C. E. Doran, and A. P. Byrne, Aust. J. Phys. **40** (1987).

[22] J. Leske, K.-H. Speidel, S. Schielke, J. Gerber, P. Maier-Komor, S. J. Q. Robinson, A. Escuderos, Y. Y. Sharon, and L.Zamick, Phys. Rev. C **74**, 024315 (2006).

[23] N. Benczer-Koller and G. J. Kumbartzki, J. Phys. G: Nucl. Part. Phys. **34**, R321 (2007).

[24] P. Maier-Komor, K.-H. Speidel, and A. Stolarz, Nucl. Instrum. Methods Phys. Res. **A 334**, 191 (1993).

[25] A. Piqué, J. M. Brennan, R. Darling, R. Tanczyn, D. Ballon, and N. Benczer-Koller, Nucl. Instrum. Methods Phys. Res. **A279**, 579 (1989).

[26] X-Ray Instrumentation Associates: `http://www.xia.com/`.

[27] G. J. Kumbartzki, K.-H. Speidel, N. Benczer-Koller, D. A. Torres, Y. Y. Sharon, L. Zamick, S. J. Q. Robinson, P. Maier-Komor, T. Ahn, V. Anagnostatou, et al., Phys. Rev. C **85**, 044322 (2012).

[28] A. Arima and F. Iachello, Phys. Rev. Lett. **35**, 1069 (1975).

[29] A. Arima and F. Iachello, Ann. Phys. (NY) **99**, 253 (1976).

[30] M. Sambataro, O. Scholten, A. Dieperink, and G. Piccito, Nucl. Phys. **A 423**, 333 (1984).

[31] I. Morrison, Aust. J. Phys. **33**, 801 (1981).

[32] A. F. Lisetskiy, B. A. Brown, M. Horoi, and H. Grawe, Phys. Rev. C **70**, 044314 (2004).